ADVANCED FUNCTIONAL MATERIALS
www.afm-journal.de

Laser-Activatible PLGA Microparticles for Image-Guided Cancer Therapy In Vivo

Yang Sun, Yanjie Wang, Chengcheng Niu, Eric M. Strohm, Yuanyi Zheng, Haitao Ran, Rongzhong Huang, Di Zhou, Yuping Gong, Zhigang Wang, Dong Wang,* and Michael C. Kolios**

Poly(lactide-co-glycolic acid) (PLGA) particles are biocompatible and biodegradable, and can be used as a carrier for various chemotherapeutic drugs, imaging agents and targeting moieties. Micrometer-sized PLGA particles were synthesized with gold nanoparticles and DiI dye within the PLGA shell, and perfluorohexane liquid (PFH) in the core. Upon laser irradiation, the PLGA shell absorbs the laser energy, activating the liquid core (liquid conversion to gas). The rapidly expanding gas is expelled from the particle, resulting in a microbubble; this violent process can cause damage to cells and tissue. Studies using cell cultures show that PLGA particles phagocytosed by single cells are consistently vaporized by laser energies of 90 mJ cm^{-2}, resulting in cell destruction. Rabbits with metastasized squamous carcinoma in the lymph nodes are then used to evaluate the anti-cancer effects of these particles in the lymph nodes. After percutaneous injection of the particles and upon laser irradiation, through the process of optical droplet vaporization, ultrasound imaging shows a significant increase in contrast in comparison to the control. Histology and electron microscopy confirm damage with disrupted cells throughout the lymph nodes, which slows the tumor growth rate. This study shows that PLGA particles containing PFC liquids can be used as theranostic agents in vivo.

1. Introduction

Perfluorocarbon (PFC) liquids are chemically and biologically inert and can be made into nano- or micrometer-sized emulsions for intravascular circulation.[1–3] Upon acoustic sonification of sufficient pressure, the PFC emulsion can be vaporized using acoustic droplet vaporization (ADV).[4–8] The gas bubbles generated using ADV can be used as either intravascular ultrasound contrast agents or for cancer therapy via targeted drug delivery and mechanical cancer cell destruction.[9–15] Normally, ultrasound cannot effectively penetrate gaseous enclosures in the human body, such as bones and lungs. Also, in order to vaporize the particles large peak negative ultrasound pressures are necessary which may cause damage to the normal surrounding tissue.[16–19] PFC liquids can also be vaporized via optical irradiation, using a method called optical droplet vaporization (ODV).[20–22] Liquid PFCs have negligible absorption in the visible/near IR wavelengths, therefore gold nanoparticles are incorporated into the PFC particles to facilitate vaporization when irradiated with a laser of the appropriate wavelength and sufficient intensity. Any optically absorbing material could be used to facilitate vaporization.[23–28]

Liquid emulsions typically use a soft shell such as lipids or albumin for encapsulation. A disadvantage to using a soft shell is droplet stability; the droplets may vaporize spontaneously causing vessel occlusion.[29] The PLGA shell prevents spontaneous vaporization, and dyes or particles can be embedded within the shell during fabrication. PLGA nano and microparticles have been used in applications such as drug delivery vehicles[10,30,31] and as photoacoustic,[22,32] ultrasound[33,34] and MRI contrast agents.[35,36]

This study investigates the effectiveness of PLGA particles loaded with perfluorohexane (PFH, molecular formula C_6F_{14}) in the core, and DiI dye and gold nanoparticles (AuNPs) contained within the shell as theranostic agents: as contrast agents and for cancer therapy in vivo. The particles can potentially be used as photoacoustic contrast agents to first ensure localization within the target volume.[37–39] Upon vaporization via laser irradiation, the therapeutic effect can be achieved either with direct mechanical disruption of the targeted tissues or with the delivery of a therapeutic payload. Moreover, the bubbles formed enhance ultrasound imaging. The particles can therefore potentially be used as a contrast agent before and after the therapeutic intervention: initially as a photoacoustic contrast

Dr. Y. Sun, Dr. C. Niu, Prof. Y. Zheng, Prof. H. Ran, Dr. R. Huang, Dr. D. Zhou, Dr. Y. Gong, Prof. Z. Wang, Prof. D. Wang
Second Affiliated Hospital
Institute of Ultrasound Imaging
Chongqing Medical University
Linjiang Road 76, Chongqing 400010, P. R. China
E-mail: wzg62942443@163.com; wang57554@163.com
Y. Wang, Dr. E. M. Strohm, Prof. M. C. Kolios
Department of Physics
Ryerson University
Toronto, Ontario M5B 2K3, Canada
E-mail: mkolios@ryerson.ca

DOI: 10.1002/adfm.201402631

© 2014 WILEY-VCH Verlag GmbH & Co. KGaA, Weinheim

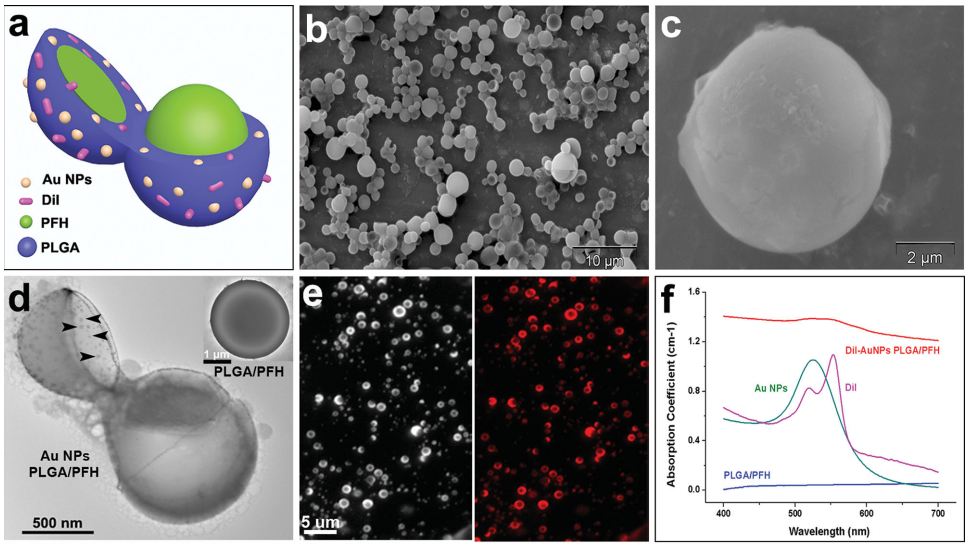

Figure 1. Morphology, structure and the absorption coefficient of the PLGA particles. a) Schematic illustration of the structure of DiI/AuNPs PLGA/PFH particle; b,c) SEM images of PLGA/PFH particles with different magnifications; d) TEM image shows the location of gold nanoparticles in PLGA shell (Au-PLGA/PFH, black arrows indicate the gold nanoparticles) (inset: a PLGA/PFH particle without AuNP for reference). e) Fluorescence images showing the dye distribution of DiI/AuNP PLGA/PFH particles under fluorescence microscopy; f) The measured optical absorption from DiI/AuNP-PLGA/PFH particles, AuNPs, DiI, and PLGA/PFH particles as control.

agent with the laser power is below the particle vaporization threshold (prior to ODV) to confirm delivery of the particles to the targeted area, and then as an ultrasound contrast agent to confirm that ODV occurred in the targeted region. In this work the particle effectiveness was investigated first in cell cultures to improve the particle configuration and laser exposure parameters. The effectiveness of the particles for cancer therapy was then investigated in vivo in rabbit metastatic lymph nodes over a seven day treatment period and compared to controls.

2. Results

2.1. Characterization of PLGA Particles

Micrometer-sized PLGA particles containing a liquid PFH core, and DiI/AuNPs within the shell were fabricated (see schematic, **Figure 1**A). SEM images of the PLGA/PFH particles are shown in Figure 1B,C. The particle morphology is generally spherical, with an average particle size of 2.5 ± 0.8 μm and shell thickness of 109 ± 32 nm, the average zeta potential of the particle was about –2.95 mV. Figure 1D shows a TEM image of particle after vaporization had occurred, with a portion of the particle shell disrupted. This image also suggests that the particle is hollow, with the AuNPs visible within the particle shell as black dots. The figure inset shows a PLGA particle without AuNPs for comparison, and the black dots are not visible. The encapsulation rate for AuNPs and PFH in the PLGA particles was approximately 23% and 55%. Figure 1E shows a fluorescent image of the particles, indicating the DiI was present in the particle shell.

The absorption coefficient of the PLGA/PFH particles with and without DiI/AuNPs are shown in Figure 1F. At 532 nm, the absorption coefficient of the PLGA particles with DiI/AuNPs was about 1.4 cm^{-1}, and negligible absorption without DiI/AuNPs. Incorporating the dye and nanoparticles into the PLGA particle increased the absorption coefficient. The optical absorption of the particles is determined by the DiI dye and AuNP concentration in the particle shell.

2.2. Particles in Cell Culture

Tests using single DiI/AuNP-loaded PLGA/PFH particles deposited onto a glass substrate were performed using a SASAM photoacoustic microscope to examine the ODV thresholds.[40] A pulsed 532 nm laser was focused onto single PLGA particles, and the laser energy was gradually increased until vaporization occurred. Optical and fluorescence images were recorded before and after vaporization. A video showing vaporization of a single 8 μm diameter particle is included in the Supporting Information (Video 1). Upon irradiation, the liquid inside the particle vaporized and escaped the PLGA particle. Within the first second, the bubble rapidly expanded to 38 μm, then slowly expanded to 50 μm over the next 12 s. The original PLGA particle remnants were clearly visible adjacent to the expanding bubble. The energy required for vaporization was typically 90 mJ cm^{-2}.

Cell uptake and the vaporization threshold of the DiI/AuNP-loaded PLGA particles were examined using MDA-MB-231 breast cancer cells. **Figure 2**A–C shows optical and fluorescence images of cells cultured with 50 μg mL^{-1} of DiI/AuNP-PLGA particles after 2 hours. The cells were stained with Hoechst to mark the nucleus (blue fluorescence), FITC to mark the cytoplasm (green fluorescence) and then the cells were observed under red fluorescence to view the DiI-stained PLGA particles. Orange is the superposition of green and red (cytoplasm and DiI-labeled particles). Particles of various sizes were observed in both the fluorescent and optical images. To confirm that the particles were internalized within the cell and not on the cell

© 2014 WILEY-VCH Verlag GmbH & Co. KGaA, Weinheim

DOI: 10.1002/adfm.201402631

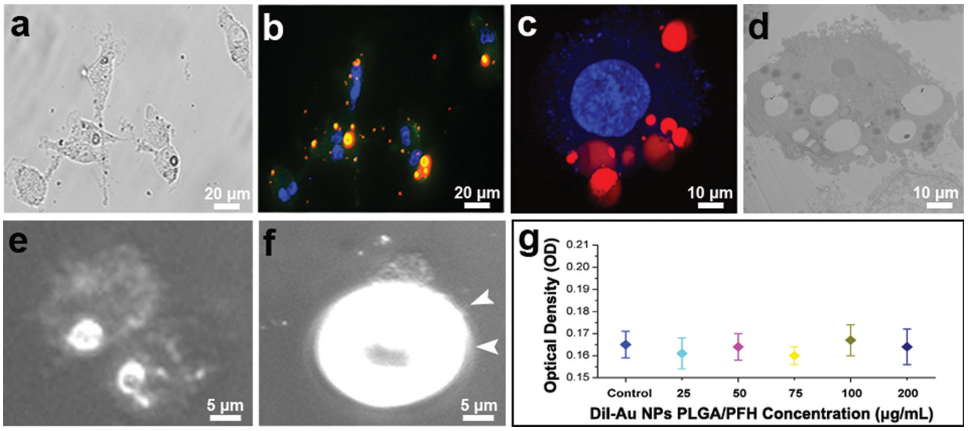

Figure 2. MDA cells were incubated with DiI/AuNP PLGA/PFH particles for 2 hours, and then the cells were stained with fluorescence dye. a) Light microscopy image of DiI/AuNP particles within MDA cells. b) A merged fluorescence image of the particles within MDA cells; blue is Hoechst marking the nucleus, green is FITC marking the cytoplasm, and red is DiI showing the PLGA particle location. The PLGA particles within the cell are orange, which is due to the superposition of the green (FITC) and red (FITC) fluorescence. c) A confocal microscopy image of MDA cells incubated with DiI-labeled PLGA/PFH particles; blue is Hoechst marking the nucleus and red is DiI marking the PLGA particles within the cell; d) A TEM image of MDA cells incubated with Au- PLGA/PFH particles; e,f) Optical image of two cells containing PLGA particles before and after vaporization. The white arrows indicate the bubble immediately after vaporization; g) Cell viability analysis after incubation with different DiI/AuNP PLGA/PFH particles concentrations.

membrane, confocal microscopy was performed on fixed cells. Figure 2C shows confocal microscopy images of a single cell stained with DAPI to stain the nucleus (blue fluorescence); the DiI-dyed particles are visible under red fluorescence. A video showing a 3D view of a rotating cell is available in the Supporting Information (Video 2). The imaging results confirm that the particles were phagocytized and internalized by the cell. The distribution of the particles in the cytoplasm were examined using TEM imaging (Figure 2D). The particles eventually escaped from the lysosome and into the cytoplasm. Cytotoxicity tests were performed to determine if the internalized PLGA particles affected cell viability.[41] The MTT assay (Figure 2G) indicates no change in optical density using particle concentrations ranging from 0 (control) to 200 μg mL^{-1}.

The ODV threshold and effects due to vaporization were examined on live cells cultured with the particles. Figure 2E,F shows optical images before and after vaporization of a particle contained with a cell. Optical contrast was poor due to low light levels within the photoacoustic microscope. Consistent particle vaporization was observed using 90 mJ cm^{-2}. Immediately after vaporization, the bubble expanded within the cell, and the cell was destroyed by the expanding bubble. Neighboring cells that did not contain particles were not affected by the bubble expansion.

2.3. In Vitro Gel Experiments

The potential of DiI/AuNP-loaded PLGA/PFH particles as contrast agents for ultrasound imaging was assessed in vitro using an agar gel model. A gel phantom 0.5 cm in diameter was made using 1% agar (w/v) dissolved in de-ionized water. An Eppendorf tube was placed in the center of the phantom to create a void where the PLGA particle solution was deposited. A solution of 100 μg mL^{-1} PLGA particles in saline was added to the central void. Measurements using standard B-mode ultrasound imaging and contrast-enhanced ultrasound (MyLab 90, Esaote, Italy) were performed on three different groups: A) A control containing only saline with no PLGA particles, B) PLGA particles without DiI/AuNPs, and C) DiI-AuNPs-loaded PLGA particles. After irradiation with a pulsed 532 nm laser using 150 mJ cm^{-2} for 5 s (Nd:YAG Q5, Leifei Shi, Beijing, China), ultrasound B-mode and contrast enhanced ultrasound imaging (CEUS) B-mode images using a 12 MHz probe were measured from each group (**Figure 3**). No difference before and after laser irradiation was observed for groups A and B. A significant increase in the ultrasound backscatter signals were observed for group C after laser irradiation (Figure 3B,C). The particles were vaporized, resulting in a solution of microbubbles. The increase in signal was due to the echogenicity of the gas bubbles in comparison to the liquid-filled PLGA/PFH particles. These measurements demonstrate that particle vaporization can be initiated and observed through a tissue-mimicking phantom using a standard clinical laser and ultrasound imaging devices.

2.4. In Vivo Experiments: Particle Vaporization and Ultrasound Contrast Enhancement

To determine if ultrasound imaging could be used to detect the vaporization of PLGA particles in vivo, animal experiments were performed. A total of 15 rabbits inoculated with the VX2 tumor line (squamous carcinoma) were divided into three groups of five, with each group receiving a different particle solution as described in section 2.3. Group A received a saline solution without any particles, group B received a 100 μg mL^{-1} solution of PLGA particles that did not contain DiI or AuNPs, and group C received a saline solution containing 100 μg mL^{-1} of DiI/AuNP-loaded PLGA/PFH particles. In all groups particle concentration was 1×10^8/mL. The rabbits were fixed in prone position, then the popliteal fossa of the rabbits were depilated

© 2014 WILEY-VCH Verlag GmbH & Co. KGaA, Weinheim

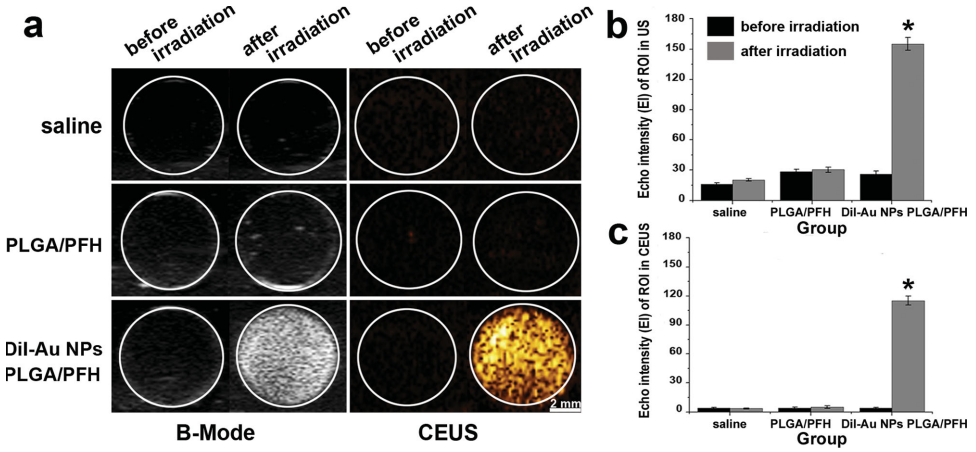

Figure 3. a) B-Mode and contrast enhanced ultrasound (CEUS) imaging of particles before and after laser irradiation in vitro (gel model) for saline only (top row), PLGA particles without DiI or AuNPs (middle row) and PLGA particles with DiI/AuNPs (bottom row). b,c) Echo intensity (EI) of the region of interest before and after laser irradiation. Echo intensity from the region of interest shown in (b), and using CEUS in (c).

with 8% Na_2S solution, and the lymph nodes were 2 mm underneath the skin. Ultrasound B-mode and CEUS-mode images of the lymph nodes were recorded 30 minutes after contrast agent administration (**Figure 4**A). The lymph nodes were then irradiated with a 532 nm laser using 150 mJ cm^{-2} for 10 s, then ultrasound B-mode and CEUS-mode images were recorded again. The ultrasound images of group A and B did not show ultrasound signal enhancement after laser irradiation. However, in group C, a significant increase in contrast was observed. The enhanced contrast due to the vaporization was detected in all 5 animals, and the average contrast enhancement is reported in Figure 4B,C.

2.5. In Vivo Experiments: Anti-Cancer Therapy

The PLGA particles were then investigated as anti-cancer therapy agents. A total of 15 rabbits containing the VX2 tumor line were divided into three groups again as described previously. Ultrasound B-mode images of the lymph node, including a blood perfusion map, were acquired on day one (prior to therapy) to measure a baseline (**Figure 5**). After imaging, the rabbits were injected with the particle solution. The area was irradiated with a 532 nm laser using 180 mJ cm^{-2} for one minute, 30 min after the particle injection. After two days, ultrasound images were recorded and the PLGA particles were injected and irradiated again. This process of ultrasound imaging before the laser irradiation was performed on days 1, 3 and 5. Ultrasound imaging was performed on day 7, then the animals were sacrificed and tumors excised for staining. In total, the lymph nodes were irradiated three times, and ultrasound imaging was performed four times; once before each laser treatment and then two days after the final treatment. Typical images of the lymph nodes, hematoxylin and eosin (H&E) staining and staining for proliferating cell nuclear antigen (PCNA) are shown in Figure 5. In group A and B, an increase in lymph node size was observed with an average volume growth rate of 69.5% and 70%, with the lymph node dimensions determined using ultrasound imaging. There was no significant differences in lymph node

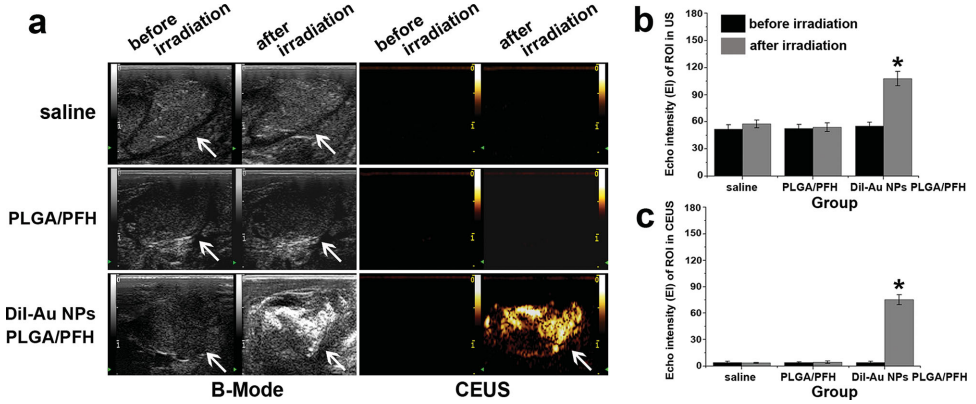

Figure 4. a) B-Mode and contrast enhanced ultrasound (CEUS) imaging of particles before and after laser irradiation in vivo for saline only (top row), PLGA particles without DiI or AuNPs (middle row) and PLGA particles with DiI/AuNPs (bottom row). The white arrows indicate the lymph nodes. b,c) Echo intensity (EI) of the region of interest before and after laser irradiation. Echo intensity from the region of interest shown in (b), and using CEUS in (c). White arrows indicate the tumor lymph nodes.

© 2014 WILEY-VCH Verlag GmbH & Co. KGaA, Weinheim

DOI: 10.1002/adfm.201402631

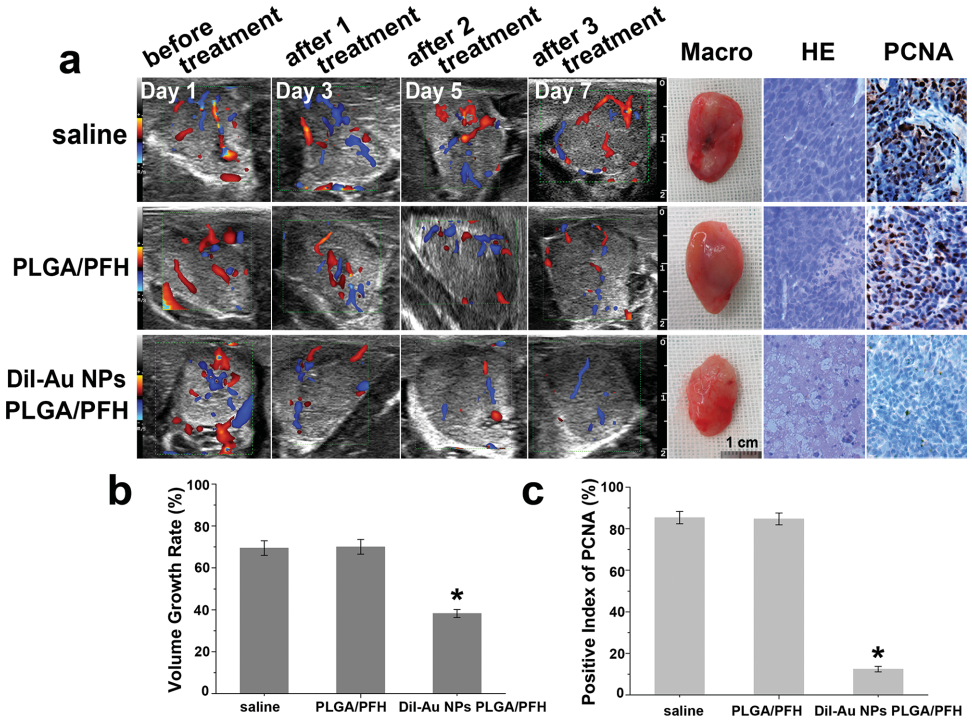

Figure 5. a–c) Ultrasound imaging of tumor lymph node on days 1 (prior to therapy), 3, 5, and 7 (after therapy). Photographs of the excised lymph node, H&E stain, PCNA expression of the tumor lymph node on day 7 after therapy. d) The volume growth rate of tumor lymph nodes in different groups after laser irradiation (*$P < 0.05$). e) PI of PCNA in different groups after laser irradiation (*$P < 0.05$).

size determined by ultrasound imaging compared to the size measured after resection of the lymph nodes ($p < 0.05$). In group C, the lymph node growth rate of 38.2% was significantly lower than group A or B ($p < 0.05$), and blood perfusion within the lymph node was reduced at day 7. No changes in body weight for any group were observed during the treatment.

The lymph nodes were sectioned and stained with H&E and PCNA-marker (Figure 5). In group A and B, no tissue damage or necrosis was apparent under H&E staining. The positive index of PCNA was 85.3% and 84.7%, indicating that the tumor lymph nodes were not affected by the treatment. In group C, damage was observed in the H&E stains, with necrosis, lysed cells and fragmented cellular and nuclear membranes visible. The expression of PCNA was absent or reduced in the necrotic region. The positive index of PCNA was 12.4% ($p < 0.05$) compared to the control. TEM imaging was used to examine damage to the cells in each group (**Figure 6**). TEM images of the lymph nodes at day 21 after tumor implantation (but prior to treatment) showed both lymph cells (white arrows) and tumor cells (black arrows), confirming tumor metastases (Figure 6A). Sections from lymph nodes from animals from group A and B appeared similar to the control with intact cellular and nuclear membranes (Figure 6B,C). Figure 6D shows typical results from group C, where significant damage to the cellular and nuclear membranes was observed (red arrows), with lysis occurring in some cells. In addition, red blood cells were observed within the tumor parenchyma (blue arrows).

3. Discussion

A new class of theranostic agents have been developed that can be used in multiple capacities: a) as a therapeutic agent, that undergoes phase conversion after laser exposure to produce a therapeutic effect, and b) as an ultrasound contrast agent that can be used after the phase conversion to validate the therapeutic delivery. The PLGA/PFH particles have been developed with AuNPs (to provide optical absorption and to aid in vaporization) and DiI (for fluorescence imaging and to aid vaporization). The dye and NPs are contained within the particle shell, and the PFH liquid within the core. The particles are small enough to circulate within the vasculature, then vaporize when irradiated with sufficient laser energy; this process is called optical droplet vaporization (ODV). The enhanced ultrasound echogenicity of the particles after vaporization confirms the liquid to gas conversion and therefore successful therapeutic deployment. In these proof of principle experiments, we have shown that phase conversion can be achieved in vivo with confirmation via ultrasound imaging. The vaporization is achieved with laser light, and therefore avoids the known limitations associated with ultrasound methods of activation.[42] We have also shown that the process of vaporization itself can create a reduction in tumor growth rates without any drug deployment.

In cell culture models, confocal microscopy confirmed that the particles were internalized by the cells. When the cells were irradiated, the vaporization process and bubble expansion destroyed critical cell structures, inducing cell death. Particle vaporization can be achieved even when the particles

© 2014 WILEY-VCH Verlag GmbH & Co. KGaA, Weinheim

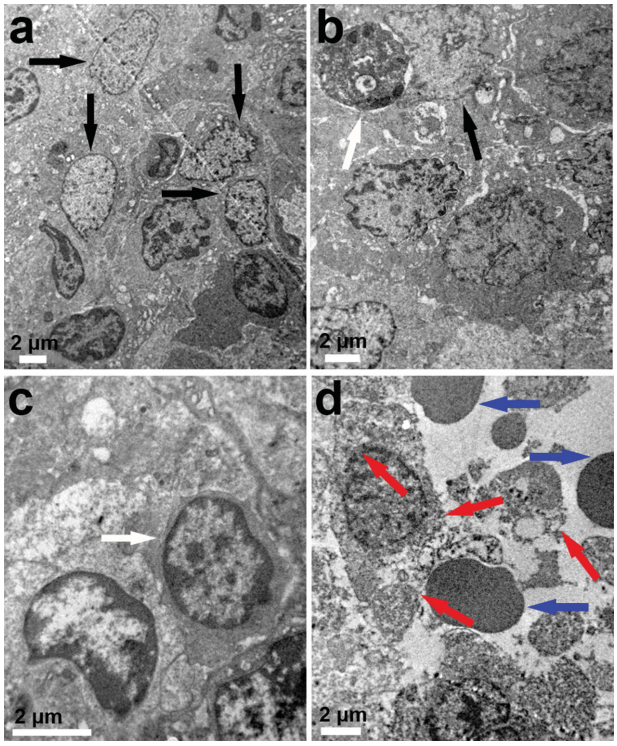

Figure 6. a) TEM image of tumor lymph nodes at 21 d after tumor implantation of the control. b–d) TEM images of the tumor lymph nodes on day 7 after the first laser irradiation. b) saline, c) PLGA/PFH particles, d) DiI/AuNPs PLGA/PFH particles. (black arrows indicate the tumor cells, white arrows indicate the lymph cells, red arrows indicate the interrupted cell membranes and nuclear membranes, blue arrows indicate the red blood cells, scale bar is 2 μm).

have been internalized within a cell; the bubble expansion is not completely suppressed by the intracellular structure. Even though the particles were generally larger than one micrometer, they can be readily phagocytosed by the MDA-MB-231 cells. Micrometer-sized particles were used in this work to visualize the particles using optical microscopy. We are currently optimizing the AuNP properties,[43] and have started the production of DiI/AuNP-PLGA particles that are 200 nm in diameter. It is expected that such particles will be able to better penetrate the endothelial barrier of blood vessels due to the enhanced permeability and retention (EPR) effect.[44]

To determine whether particle conversion could be achieved in vivo, animal experiments were performed in a rabbit VX2 tumor metastatic model. DiI/AuNP-PLGA/PFH particles were injected in the foot pad of the hind leg. Ultrasound imaging of the rabbit lymph nodes after laser exposure showed an increase in ultrasound contrast compared to before laser exposure. No change in contrast after laser irradiation was observed for the controls using saline and PLGA particles without DiI/AuNPs. The DiI/AuNP-PLGA particles underwent a phase transition, in vivo, confirmed by ultrasound imaging (Figure 4). The intravascular particles used will not typically diffuse into the tumor parenchyma without breaching the tumor blood vessels. Nevertheless, the particles did achieve a therapeutic effect, likely due to vascular stasis and direct mechanical damage to tissue. This is consistent with vascular occlusion due to acoustic droplet vaporization reported by Kripfgans et al.[29]

The effects of the PLGA particles for anti-cancer treatment was tested in vivo on rabbit lymph nodes containing metastases. The metastatic nodes treated with the DiI/AuNP-PLGA particles showed a significant decrease in growth volume compared to the control and the PLGA particles without DiI/AuNPs. At day 3 (after one treatment), the ultrasound images and perfusion maps were similar to day 1, prior to treatment. At days 5 and 7 (after two and three treatments, respectively), significant voids were observed in the ultrasound images, attributed to tissue damage and necrosis. Blood flow was also reduced within the lymph node. The treatment using saline and PLGA particles without DiI/AuNPs showed no significant changes throughout the treatment. No weight changes or adverse effects on the rabbits were observed throughout the seven-day treatment. H&E stained sections showed damage and the treated sections had reduced PCNA staining, and thus cancer cell proliferation. TEM imaging revealed extensive damage to the cellular network of the lymph nodes treated with the DiI/AuNP-PLGA particles. Broken cellular and nuclear membranes, as well as the presence of red blood cells were observed in the tissue. Due to their large size, the PLGA particles were likely restricted to within the vascular/lymph network, as sizes <200 nm are typically required to penetrate the endothelial cells. The presence of red blood cells indicates that the vasculature was damaged, enabling the particles and blood cells to flow into the tumor parenchyma. As the treatment progressed, further damage to the tissue occurred. Another potential bioeffect that would impact tumor cell proliferation is that of ultraosund induced cancer immunotherapy. The destruction of tumor cells in the lymph nodes may lead to immunity forming in situ by immune cells being exposed to the cancer cell reminants, whose response is potentially amplified when the exposures are in the lymph node.[45]

In conclusion, this study shows that these newly developed PLGA particles can be used as theranostic agents. The particles can be selectively vaporized within a region of interest to destroy tissue, and enhance the ultrasound contrast. The particle effectiveness as an anti-cancer therapy can be enhanced by adding a drug payload into the particle core alongside the PFH liquid. Such an approach has been used in emulsions by other investigators.[11,46] Upon vaporization, the drug would be expelled into the region. A high dose would be concentrated at the target area, minimizing systemic side effects. The particle surface could be functionalized with common cancer-proteins to preferentially bind to cancer cells, further increasing the probably of damaging cancer cells. Further work is required to examine the particle kinetics, such as circulation time, particle biodistribution, and any adverse affects with administration of these agents. Studies comparing the effects of PLGA particles to PFC droplets on single cells are planned to determine the necrosis mechanism.

Supporting Information

Supporting Information is available from the Wiley Online Library or from the author.

© 2014 WILEY-VCH Verlag GmbH & Co. KGaA, Weinheim
Adv. Funct. Mater. **2014**,
DOI: 10.1002/adfm.201402631

Acknowledgements

The authors thank Chester Santiago, Elizabeth Berndl, and Arthur Worthington (Ryerson University), and Pan Li (Chongqing Medical University) for their technical assistance. This project was funded by the National Nature Science of China (Grant No. 81130025, 81401423, 81227801, 81161120548, 81371579, 31300137) and Chongqing University Innovation Team Plans (KJTD201303) and the Canadian Institutes of Health Research (CCI-249368). Funding to purchase the equipment was provided by the Canada Foundation for Innovation, the Ontario Ministry of Research and Innovation, and Ryerson University.

Received: August 4, 2014
Revised: August 31, 2014
Published online:

[1] N. Rapoport, *Wiley Interdiscip. Rev. Nanomed. Nanobiotechnol.* **2012**, *4*, 492.
[2] J. Huang, J. S. Xu, R. X. Xu, *Biomaterials* **2010**, *31*, 1278.
[3] J.-M. Lu, X. Wang, C. Marin-Muller, H. Wang, P. H. Lin, Q. Yao, C. Chen, *Expert Rev. Mol. Diagn.* **2009**, *9*, 325.
[4] O. D. Kripfgans, J. B. Fowlkes, D. L. Miller, O. P. Eldevik, P. L. Carson, *Ultrasound Med. Biol.* **2000**, *26*, 1177.
[5] P. S. Sheeran, S. H. Luois, L. B. Mullin, T. O. Matsunaga, P. A. Dayton, *Biomaterials* **2012**, *33*, 3262.
[6] N. Reznik, O. Shpak, E. C. Gelderblom, R. Williams, N. de Jong, M. Versluis, P. N. Burns, *Ultrasonics* **2013**, *53*, 1368.
[7] Y. Zhou, Z. Wang, Y. Chen, H. Shen, Z. Luo, A. Li, Q. Wang, H. Ran, P. Li, W. Song, Z. Yang, H. Chen, Z. Wang, G. Lu, Y. Zheng, *Adv. Mater.* **2013**, *25*, 4123.
[8] O. Shpak, M. Verweij, H. J. Vos, N. de Jong, D. Lohse, M. Versluis, *Proc. Natl. Acad. Sci.* USA **2014**, *111*, 1697.
[9] C.-H. Wang, S.-T. Kang, Y.-H. Lee, Y.-L. Luo, Y.-F. Huang, C.-K. Yeh, *Biomaterials* **2012**, *33*, 1939.
[10] M. L. Fabiilli, J. a Lee, O. D. Kripfgans, P. L. Carson, J. B. Fowlkes, *Pharm. Res.* **2010**, *27*, 2753.
[11] N. Y. Rapoport, A. M. Kennedy, J. E. Shea, C. L. Scaife, K.-H. Nam, *J. Controlled Release* **2009**, *138*, 268.
[12] R. Williams, C. Wright, E. Cherin, N. Reznik, M. Lee, I. Gorelikov, F. S. Foster, N. Matsuura, P. N. Burns, *Ultrasound Med. Biol.* **2013**, *39*, 475.
[13] P. S. Sheeran, V. P. Wong, S. Luois, R. J. McFarland, W. D. Ross, S. Feingold, T. O. Matsunaga, P. A. Dayton, *Ultrasound Med. Biol.* **2011**, *37*, 1518.
[14] S.-T. Kang, C.-K. Yeh, *Langmuir* **2011**, *27*, 13183.
[15] D. Kagan, M. J. Benchimol, J. C. Claussen, E. Chuluun-Erdene, S. Esener, J. Wang, *Angew. Chem.* **2012**, *124*, 7637.
[16] E. M. Knavel, C. L. Brace, *Tech. Vasc. Interv. Radiol.* **2013**, *16*, 192.
[17] A. D. Maxwell, T.-Y. Wang, L. Yuan, A. P. Duryea, Z. Xu, C. A. Cain, *Ultrasound Med. Biol.* **2010**, *36*, 2132.
[18] C.-K. Yeh, *Chang Gung Med. J.* **2012**, *35*, 125.
[19] M. Zhang, M. L. Fabiilli, K. J. Haworth, F. Padilla, S. D. Swanson, O. D. Kripfgans, P. L. Carson, J. B. Fowlkes, *Acad. Radiol.* **2011**, *18*, 1123.
[20] E. M. Strohm, M. Rui, M. C. Kolios, I. Gorelikov, N. Matsuura, in *IEEE Int. Ultrason. Symp.*, IEEE, San Diego, USA **2010**, 495–498.
[21] E. M. Strohm, M. Rui, I. Gorelikov, N. Matsuura, M. Kolios, *Biomed. Opt. Express* **2011**, *2*, 1432.
[22] K. Wilson, K. Homan, S. Emelianov, *Nat. Commun.* **2012**, *3*, 618.
[23] H. J. Lee, Y. Liu, J. Zhao, M. Zhou, R. R. Bouchard, T. Mitcham, M. Wallace, R. J. Stafford, C. Li, S. Gupta, M. P. Melancon, *J. Controlled Release* **2013**, *172*, 152.
[24] G. Ku, M. Zhou, S. Song, Q. Huang, J. Hazle, C. Li, *ACS Nano* **2012**, *6*, 7489.
[25] J. V. Jokerst, M. Thangaraj, P. J. Kempen, R. Sinclair, S. S. Gambhir, *ACS Nano* **2012**, *6*, 5920.
[26] B. S. Gutrath, M. F. Beckmann, A. Buchkremer, T. Eckert, J. Timper, A. Leifert, W. Richtering, G. Schmitz, U. Simon, *Nanotechnology* **2012**, *23*, 225707.
[27] B. Wang, Q. Zhao, N. M. Barkey, D. L. Morse, H. Jiang, *Med. Phys.* **2012**, *39*, 2512.
[28] D. Pan, B. Kim, L. V. Wang, G. M. Lanza, *Wiley Interdiscip. Rev. Nanomed. Nanobiotechnol.* **2013**, *5*, 517.
[29] M. Zhang, M. L. Fabiilli, K. J. Haworth, J. B. Fowlkes, O. D. Kripfgans, W. W. Roberts, K. A. Ives, P. L. Carson, *Ultrasound Med. Biol.* **2010**, *36*, 1691.
[30] N. Rapoport, K.-H. Nam, R. Gupta, Z. Gao, P. Mohan, A. Payne, N. Todd, X. Liu, T. Kim, J. Shea, C. Scaife, D. L. Parker, E.-K. Jeong, A. M. Kennedy, *J. Controlled Release* **2011**, *153*, 4.
[31] J. Kim, J. E. Lee, S. H. Lee, J. H. Yu, J. H. Lee, T. G. Park, T. Hyeon, *Adv. Mater.* **2008**, *20*, 478.
[32] A. Hannah, G. Luke, K. Wilson, K. Homan, S. Emelianov, *ACS Nano* **2014**, *8*, 250.
[33] E. Pisani, N. Tsapis, J. Paris, V. Nicolas, L. Cattel, E. Fattal, *Langmuir* **2006**, *22*, 4397.
[34] R. X. Xu, *Contrast Media Mol. Imaging* **2011**, *6*, 401.
[35] M. Srinivas, L. J. Cruz, F. Bonetto, A. Heerschap, C. G. Figdor, I. J. M. de Vries, *Biomaterials* **2010**, *31*, 7070.
[36] Y. Wang, Y. W. Ng, Y. Chen, B. Shuter, J. Yi, J. Ding, S.-c. Wang, S. S. Feng, *Adv. Funct. Mater.* **2008**, *18*, 308.
[37] A. L. Doiron, K. A. Homan, S. Emelianov, L. Brannon-Peppas, *Pharm. Res.* **2009**, *26*, 674.
[38] Y. Kohl, C. Kaiser, W. Bost, F. Stracke, M. Fournelle, C. Wischke, H. Thielecke, A. Lendlein, K. Kratz, R. Lemor, *Nanomedicine* **2011**, *7*, 228.
[39] Y. Sun, Chengcheng Niu, Yanjie Wang, Eric M. Strohm , Haitao Ran, Yuanyi Zheng, Zhigang Wang, Michael C. Kolios, in *IEEE Int. Ultrason. Symp.* Prague, Czech Republic **2013**.
[40] E. M. Strohm, E. S. L. Berndl, M. C. Kolios, *Photoacoustics* **2013**, *1*, 49.
[41] C. Niu, Z. Wang, G. Zuo, T. M. Krupka, H. Ran, P. Zhang, P. Li, Y. Chen, H. Chen, Y. Zheng, *Clin. Breast Cancer* **2012**, *12*, 199.
[42] P. S. Sheeran, P. A. Dayton, *Scientifica* **2014**, *2014*, e579684.
[43] Y. J. Wang, E. M. Strohm, Y. Sun, C. Niu, Y. Zheng, Z. Wang, M. C. Kolios, in *Proc. SPIE* **2014**, 89433M–89433M–7.
[44] H. Maeda, *Adv. Enzyme Regul.* **2001**, *41*, 189.
[45] J. Unga, M. Hashida, *Adv. Drug Delivery Rev.* **2014**, *72*, 144.
[46] M. L. Fabiilli, K. J. Haworth, I. E. Sebastian, O. D. Kripfgans, P. L. Carson, J. B. Fowlkes, *Ultrasound Med. Biol.* **2010**, *36*, 1364.

© 2014 WILEY-VCH Verlag GmbH & Co. KGaA, Weinheim